

DEVELOPMENT OF AN ADAPTIVE EMPIRICAL MODEL FOR STORM TIDE SIMULATION

U Hin Lai¹, Ka In Hoi¹ and Kai Meng Mok^{1,2}

The abrupt rise in local sea level due to storm tide caused by an approaching tropical cyclone could cause severe flooding and devastating influence to low-lying regions of a coastal city. Studies show that many empirical offline modeling techniques are useful tools for storm tide simulation, e.g. the Artificial Neural Network (ANN). However, these techniques are non-adaptive and retraining is necessary when new data are available. The present study introduces an adaptive empirical model for improvement. It is a dynamic linear regression model with the harmonic tidal prediction, wind speed, wind direction and atmospheric pressure as the model input parameters. Application of the model to simulate the storm tide variation of forty tropical cyclone cases in Macau gives values of the root-mean-squared error and the coefficient of determination ranging between 0.08~0.20m and 0.82~0.98, respectively. In addition, the proposed model could capture the storm tide maxima of the seventeen flooding cases among the forty with a root-mean-squared error of 0.15m. Simulation of the corresponding peak arrival for the flooding cases is mostly within one hour of the actual one and at most two hours. Therefore, the proposed adaptive model is a promising tool for storm tide simulation.

Keywords: adaptive model; flooding; Kalman filter; storm surge; storm tide

INTRODUCTION

Tropical cyclone can cause persistent onshore winds pushing the water body towards inland (wind set-up) as well as the local sucking of water upwards near/within the low pressure center (inverted barometer effect). This surge phenomenon combines with the normal astronomical tide to form the storm tide. Storm tide could cause severe flooding and damage on coastal areas, especially the low-lying region. Therefore, modeling how the astronomical/meteorological factors contribute to the resultant storm tide is important for coastal and ocean engineers who design maritime protection structures against flooding (e.g. dikes, sea walls, etc.). In general, there are two types of storm tide simulation models, namely the deterministic model and the statistical model. Deterministic models such as SLOSH are 2D/3D hydrodynamic models that simulate the storm tide level over a large area under prescribed coastal/topographic boundary conditions and wind field (Wong and Li, 2007; Wong and Wong, 2008). However, they require high computational effort and data to setup and run.

On the other hand, statistical models are appealing to simulate the tidal level of a small urban area with significantly less computational cost and sea level/meteorological measurements of a few monitoring station. Lee (2006) used the artificial neural network (ANN) for the storm tide prediction in Taiwan. Rajasekaran et al. (2008) performed similar application by applying the support vector regression (SVR). However, the learning algorithms in these studies are offline, meaning that those models are non-adaptive and retraining is necessary when new data are available. Therefore, the objective of this study is to introduce an adaptive statistical model for improvement. The model adaptiveness is fulfilled by the time varying model coefficients estimated by the Kalman filter algorithm (Kalman, 1960; Kalman and Bucy, 1961) that has broad application in the field of environmental science and engineering (Choi et al., 2002; Chao et al., 2012 and Hoi et al., 2013). The proposed methodology is tested by simulating the storm tide of forty tropical cyclone cases in Macau.

METHODOLOGY

Storm tide is basically a combination of the normal astronomical tide and the storm surge induced by a tropical cyclone. The two main meteorological factors contributing to a storm surge are the winds and the pressure drops associated with the cyclone. The pressure drop can be measured by the difference of the local atmospheric pressure p from its standard value p_0 of 1013.3hPa. Effects of the winds can be expressed as forcing in the form of an acceleration defined as w^2/AT , where w is the measured wind speed and AT is the astronomical tide prediction. As the direction of the wind forcing applied is important, the acceleration can be decomposed into an east-west component $w^2 AT^{-1} \sin \phi$ and a north-south component $w^2 AT^{-1} \cos \phi$, where ϕ is the wind direction measured clockwise from the North. The wind forcing may not be in phase with its effects on the surge. A correlation analysis between the acceleration components and the storm surge of different hours would provide good reference for model development. In this study, two cases of storm tide that caused the most severe flooding in Macau are selected for analysis. They are case 0814(HAGUPIT) and case 0915(KOPPU)

¹ Department of Civil and Environmental Engineering, Faculty of Science and Technology, University of Macau, Avenida da Universidade, Taipa, Macau, China

² Corresponding author, Email: kmmok@umac.mo

that occurred in 2008 and 2009, respectively. Table 1 shows the Pearson correlation coefficient (R) between the acceleration components of the k^{th} hour and the measured storm surge SS at the k^{th} hour to $k+9^{\text{th}}$ hour, where SS is calculated by subtracting the astronomical tide prediction from the tide gauge measurement. It is found that both cases have similar correlation patterns (see bold numbers in Table 1). First, the east-west component of the wind forcing $w^2 AT^{-1} \sin \phi$ has already high positive correlation with the storm surge of the same hour. The correlation gets stronger as times goes by and it reaches its maximum when the time difference is three to four hours. Then, the strength of correlation declines gradually. However, there is still moderate correlation at a time difference of eight to nine hours. On the other hand, strong positive correlation between the north-south component $w^2 AT^{-1} \cos \phi$ and the storm surge starts at around $k+3^{\text{th}}$ hour and it reaches its maximum when the time difference is seven to eight hours. Through these correlation patterns, it can be concluded that the easterly winds are responsible for the wind setup of first few hours. Then, its effects dissipate gradually. In the subsequent hours, the northerly winds become the dominant factor for the wind setup. Therefore, the north-south/east-west wind acceleration components of the previous nine hours should be included in the model to reflect different stages of the wind setup process.

| Table 1. Pearson correlation coefficient (R) between the hourly storm surge and the wind forcing components with different time-lags | | | | |
|--|-------------------------------|-------------------------------|-------------------------------|-------------------------------|
| | Case 0814 | | Case 0915 | |
| | $w_k^2 AT_k^{-1} \cos \phi_k$ | $w_k^2 AT_k^{-1} \sin \phi_k$ | $w_k^2 AT_k^{-1} \cos \phi_k$ | $w_k^2 AT_k^{-1} \sin \phi_k$ |
| SS_k | -0.07 | 0.70 | -0.09 | 0.47 |
| SS_{k+1} | 0.11 | 0.82 | 0.05 | 0.65 |
| SS_{k+2} | 0.29 | 0.92 | 0.22 | 0.79 |
| SS_{k+3} | 0.46 | 0.95 | 0.38 | 0.89 |
| SS_{k+4} | 0.62 | 0.94 | 0.56 | 0.93 |
| SS_{k+5} | 0.76 | 0.89 | 0.71 | 0.89 |
| SS_{k+6} | 0.85 | 0.81 | 0.82 | 0.80 |
| SS_{k+7} | 0.90 | 0.68 | 0.89 | 0.66 |
| SS_{k+8} | 0.89 | 0.54 | 0.91 | 0.53 |
| SS_{k+9} | 0.84 | 0.40 | 0.88 | 0.39 |

The proposed Kalman filter based storm tide simulation model (STS_k) of the k^{th} hour is a linear combination of the astronomical tide prediction (AT_k) at the k^{th} hour, the measured atmospheric pressure drop ($p_0 - p_k$) at the k^{th} hour, the measured wind speed (w_{k-9} to w_k) and wind direction (ϕ_{k-9} to ϕ_k) at the $(k-9)^{\text{th}}$ hour to the k^{th} hour, and the storm surge simulation of the previous hour S_{k-1} expressed as $STS_{k-1} - AT_{k-1}$:

$$\begin{aligned}
 STS_k = & \theta_{1,k} AT_k + \theta_{2,k} (p_0 - p_k) + \theta_{3,k} WC_k + \theta_{4,k} \frac{w_{k-1} + w_{k-2} + w_{k-3}}{3} \\
 & + \theta_{5,k} \frac{w_{k-4} + w_{k-5} + w_{k-6}}{3} + \theta_{6,k} \frac{w_{k-7} + w_{k-8} + w_{k-9}}{3} + \theta_{7,k} WS_k \\
 & + \theta_{8,k} \frac{w_{k-1} + w_{k-2} + w_{k-3}}{3} + \theta_{9,k} \frac{w_{k-4} + w_{k-5} + w_{k-6}}{3} \\
 & + \theta_{10,k} \frac{w_{k-7} + w_{k-8} + w_{k-9}}{3} + \theta_{11,k} S_{k-1}
 \end{aligned} \quad (1)$$

where

$$WC_k = \frac{w_k^2 \cos \phi_k}{AT_k} \quad (2)$$

and

$$WS_k = \frac{w_k^2 \sin \phi_k}{AT_k} \quad (3)$$

In this expression, AT_k represents the astronomical tide prediction of the k^{th} hour by the following harmonic model:

$$AT_k = \mu + \sum_{i=1}^7 (A_i \cos \omega_i k + B_i \sin \omega_i k) \quad (4)$$

where μ is the mean sea level and ω_i represents the angular speed of the i^{th} dominant tidal constituent. Choi et al. (2002) showed that seven dominant constituents ($M_2, K_1, O_1, S_2, P_1, N_2$ & K_2) are sufficient to explain 86% variance of the tidal variation in Macau. Therefore, the same tidal

constituents are adopted in this study. Table 2 shows the names, diurnal characteristics, and angular speeds of these seven constituents for reference.

| Table 2. Dominant tidal constituents of Macau | | | |
|---|-----------------------|-------------------------|-----------------------------|
| Symbol | Constituent name | Diurnal characteristics | Angular speed (degree/hour) |
| M ₂ | Principal lunar | Semidiurnal | 28.9841042 |
| K ₁ | Luni-solar | Diurnal | 15.0410686 |
| O ₁ | Principal lunar | Diurnal | 13.9430356 |
| S ₂ | Principal solar | Semidiurnal | 30.0000000 |
| P ₁ | Principal solar | Diurnal | 14.9589314 |
| N ₂ | Larger lunar elliptic | Semidiurnal | 28.4397295 |
| K ₂ | Luni-solar | Semidiurnal | 30.0821373 |

Kalman filter is used to update the time-varying model coefficients $\theta_{i,k}$ in Eq. (1) every hour according to the measured sea level. For its implementation, Eq. (1) is rewritten into the form of a generalized dynamic linear model:

$$STS_k = \mathbf{C}_k \boldsymbol{\theta}_k \quad (5)$$

where STS_k denotes the predicted hourly tidal level, \mathbf{C}_k is a row vector containing the following input functions:

$$\mathbf{C}_k = \left[AT_k \quad p_0 - p_k \quad WC_k \quad \frac{\sum_{i=1}^3 WC_{k-i}}{3} \quad \frac{\sum_{i=4}^6 WC_{k-i}}{3} \quad \frac{\sum_{i=7}^9 WC_{k-i}}{3} \right. \\ \left. WS_k \quad \frac{\sum_{i=1}^3 WS_{k-i}}{3} \quad \frac{\sum_{i=4}^6 WS_{k-i}}{3} \quad \frac{\sum_{i=7}^9 WS_{k-i}}{3} \quad S_{k-1} \right] \quad (6)$$

and $\boldsymbol{\theta}_k$ is the state vector which contains the unknown model coefficients of the k^{th} hour:

$$\boldsymbol{\theta}_k = [\theta_{1,k} \quad \dots \quad \theta_{11,k}]^T \quad (7)$$

Each model coefficient of this hour is assumed to differ slightly from the coefficient of the previous one according to the pure random walk:

$$\theta_{i,k} = \theta_{i,k-1} + f_{i,k-1} \quad (8)$$

where $f_{i,k-1}$ is the variation made to the coefficient $\theta_{i,k-1}$ on the $(k-1)^{\text{th}}$ hour. It is assumed to follow a normal distribution with zero mean and a standard deviation of σ_i . Then, Eq. (8) can be rewritten as the following vector form:

$$\boldsymbol{\theta}_k = \boldsymbol{\theta}_{k-1} + \mathbf{F}_{k-1} \quad (9)$$

where \mathbf{F}_{k-1} follows a Gaussian i.i.d. vector process with zero mean and covariance matrix $\sum_{\mathbf{F}} = \text{diag}(\sigma_1^2, \dots, \sigma_{11}^2)$. To update the model coefficients, the measured hourly sea level z_k is required and it is related to the parameter vector $\boldsymbol{\theta}_k$ through the following equation:

$$z_k = \mathbf{C}_k \boldsymbol{\theta}_k + n_k \quad (10)$$

where n_k which is the modeling error. This modeling error is generally assumed as Gaussian i.i.d. with zero mean and variance σ_n^2 . The Kalman filter algorithm consists of two fundamental steps, namely the prediction step and the filtering step. First of all, the model coefficients of the k^{th} hour are predicted by

$$\boldsymbol{\theta}_{k|k-1}^* = \boldsymbol{\theta}_{k-1|k-1}^* \quad (11)$$

Eq. (11) means that the prior estimate of the model coefficients of the k^{th} hour is predicted by the posterior estimate of the $(k-1)^{\text{th}}$ hour. The uncertainties and correlations structures of the predicted model coefficients are given by the following covariance matrix:

$$\sum_{\boldsymbol{\theta},k|k-1} = \sum_{\boldsymbol{\theta},k-1|k-1} + \sum_{\mathbf{F}} \quad (12)$$

When the measurement of the k^{th} hour is available, the model coefficients can be updated by maximizing the posterior probability density function (PDF) $p(\boldsymbol{\theta}_k | \mathbf{D}_k)$ (Yuen, 2010):

$$\boldsymbol{\theta}_{k|k}^* = \sum_{\boldsymbol{\theta},k|k} \left(\sum_{\boldsymbol{\theta},k|k-1}^{-1} \boldsymbol{\theta}_{k|k-1}^* + \frac{\mathbf{C}_k^T z_k}{\sigma_n^2} \right) \quad (13)$$

The updated uncertainties and correlation structures of the model coefficients at the k^{th} hour are given by the covariance matrix $\Sigma_{\theta,k|k}$:

$$\Sigma_{\theta,k|k} = \left(\Sigma_{\theta,k|k-1}^{-1} + \frac{C_k^T C_k}{\sigma_n^2} \right)^{-1} \quad (14)$$

Figure 1 shows the flowchart of applying the Kalman filter to perform state estimation.

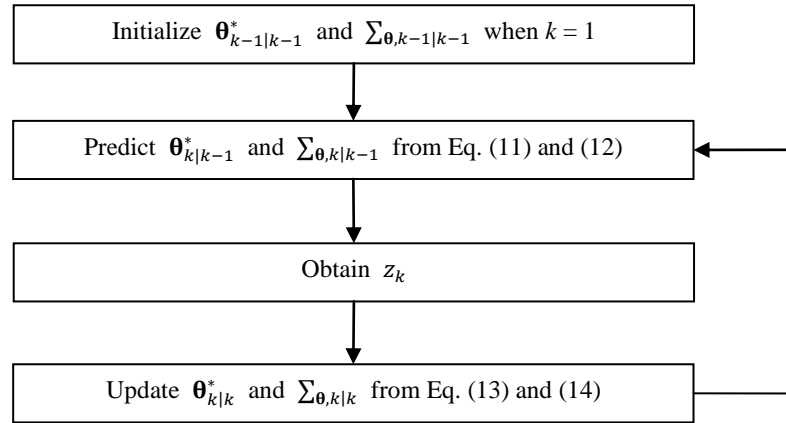


Figure 1. Kalman filter flowchart

RESULT AND DISCUSSION

During the normal period, variation of the sea level is mainly driven by the astronomical tidal motions. The harmonic model described in Eq. (4) would describe its behaviors well. Using the hourly tide gauge data recorded at the Macau inner harbor from 1985 to 2004, the mean sea level and coefficients of the seven dominant tidal constituents of Macau listed in Table 2 are determined for the harmonic model. Figure 2 shows the temporal variation of the measured sea level (solid line) together with the harmonic model prediction (blue dot) in two separate periods of September 2008. Figure 2(a) covers a normal period between 2008-09-01 00:00 and 2008-09-15 23:00. Good agreement of the predicted astronomical tide with the measurement is observed. Figure 2(b) covers a period between 2008-09-16 00:00 and 2008-09-30 23:00, in which a tropical cyclone (case 0814) passed through between 2008-09-22 22:00 to 2008-09-24 16:00. It is shown that the harmonic model fails to capture the tidal level during the period of the cyclone passing due to the presence of an induced storm surge.

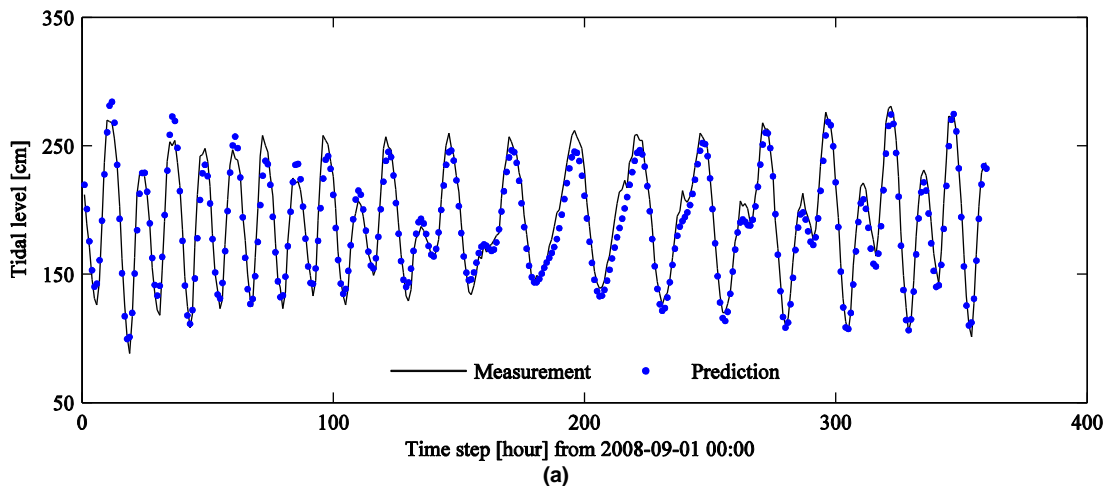


Figure 2. The measured and predicted tidal level in period of (a) 01-15/09/2008; (b) 16-30/09/2008. (Continued on the next page.)

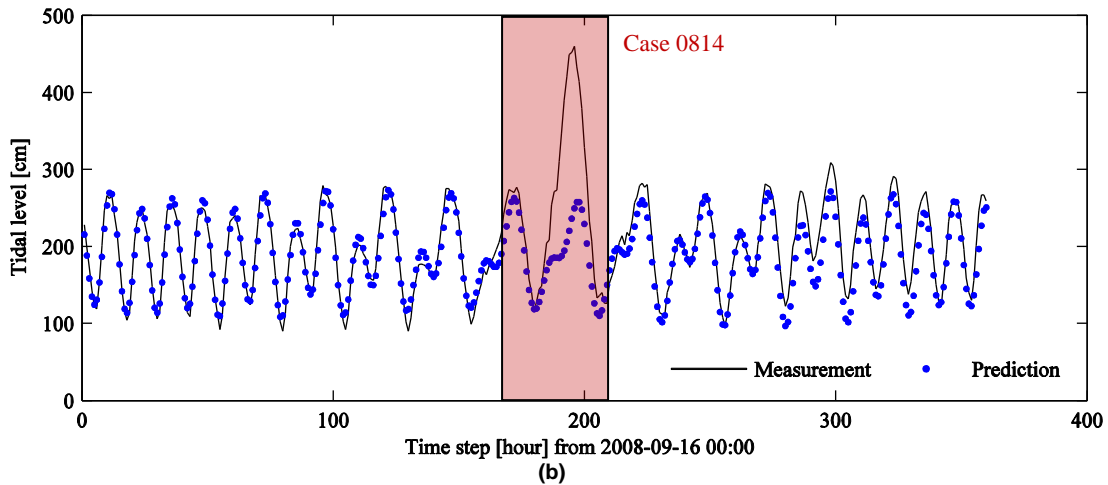


Figure 2. (continued) The measured and predicted tidal level in period of (a) 01-15/09/2008; (b) 16-30/09/2008

Typical performance of the harmonic model in a normal period and in a period with a tropical cyclone passing is demonstrated quantitatively by values of the root mean square error (*RMSE*) and the coefficient of determination (R^2) of the corresponding period shown in Table 3. It is obvious that with the presence of a tropical cyclone generated storm surge, the harmonic model gives larger (3.2 times) *RMSE* and smaller (24% lesser) R^2 . This is expected as the harmonic model does not count for the meteorological conditions that are important in affecting the sea level during the cyclone period. Therefore, a storm tide model that can handle these extra influencing factors is needed for that period.

| Date range | Period | <i>RMSE</i> (m) | R^2 |
|---------------|--------------------------|-----------------|-------|
| 01-15/09/2008 | Without tropical cyclone | 0.12 | 0.95 |
| 16-30/09/2008 | With tropical cyclone | 0.38 | 0.72 |

Figure 2(b) shows that the effect of the storm surge on steering the sea level away from its regular tidal motion does not last long. Therefore, the time for applying a storm tide model that can count for the influencing meteorological conditions should be set so that the sea level can be estimated better in that period. The warning of a threat by an approaching tropical cyclone is officially issued in Macau by the Meteorological and Geophysical Bureau (SMG). The system has five levels of warnings as shown in Table 4. In this study, the storm tide model is set to start for estimating the sea level when a warning no.1 is issued. The model is stopped when all warnings are cancelled.

| Warning | Meaning of warning |
|---------|---|
| No.1 | The center of a tropical cyclone is less than 800 km from Macau SAR and may later affect the Macau SAR. |
| No.3 | The center of a tropical cyclone follows a pattern of movement that winds to be experienced in Macau SAR may possibly range from 41 to 62 km/h and gusts about 110 km/h. |
| No.8 | The center of a tropical cyclone is nearing and winds recorded in Macau SAR may possibly range from 63 to 117 km/h with gusts reaching about 180 km/h. |
| No.9 | The center of a tropical cyclone is approaching Macau SAR and it is expected that Macau SAR might be severely affected. |
| No.10 | The center of the on-coming tropical cyclone shall strike at the immediate approaches of Macau SAR. The mean wind speed should exceed 118 km/h with gusts of great intensity. |

The atmospheric pressure and the wind velocity data used are measured by a weather station installed at Taipa Grande (TG) where SMG is located. There were forty cases of tropical cyclone in Macau between 2005 and 2012. The *STS* model is applied to simulate the storm tidal level of them. As the effect of a tropical cyclone on the sea level may vary due to the strength and traveling track of the cyclone, cases with the same highest warning issued are grouped together for analysis. The results of *RMSE* and R^2 are summarized in Table 5. It appears that there is not much difference in model performance regardless the highest tropical cyclone warning issued. This means that the proposed *STS* model can handle a wide range of tropical cyclone condition (warning no.1 to no.9) with its adaptive nature.

| Highest warning issued | No. of cases | <i>RMSE</i> (m) | | | | R^2 | | | |
|------------------------|--------------|-----------------|------|---------|--------------------|-------|------|---------|--------------------|
| | | Min. | Max. | Average | Standard deviation | Min. | Max. | Average | Standard deviation |
| No.1 | 15 | 0.08 | 0.16 | 0.12 | 0.02 | 0.82 | 0.97 | 0.94 | 0.05 |
| No.3 | 14 | 0.08 | 0.16 | 0.12 | 0.02 | 0.88 | 0.98 | 0.94 | 0.03 |
| No.8 | 10 | 0.09 | 0.20 | 0.14 | 0.03 | 0.90 | 0.98 | 0.94 | 0.03 |
| No.9 | 1 | - | - | 0.14 | - | - | - | 0.96 | - |

Temporal variation of the storm tide level given by the model simulation with measurements for two cases with the highest and lowest *RMSE* of each group listed in Table 5 are shown in Figure 3 to Figure 6. In general, the model simulations could capture the storm tide variations well in all cases of different cyclone conditions.

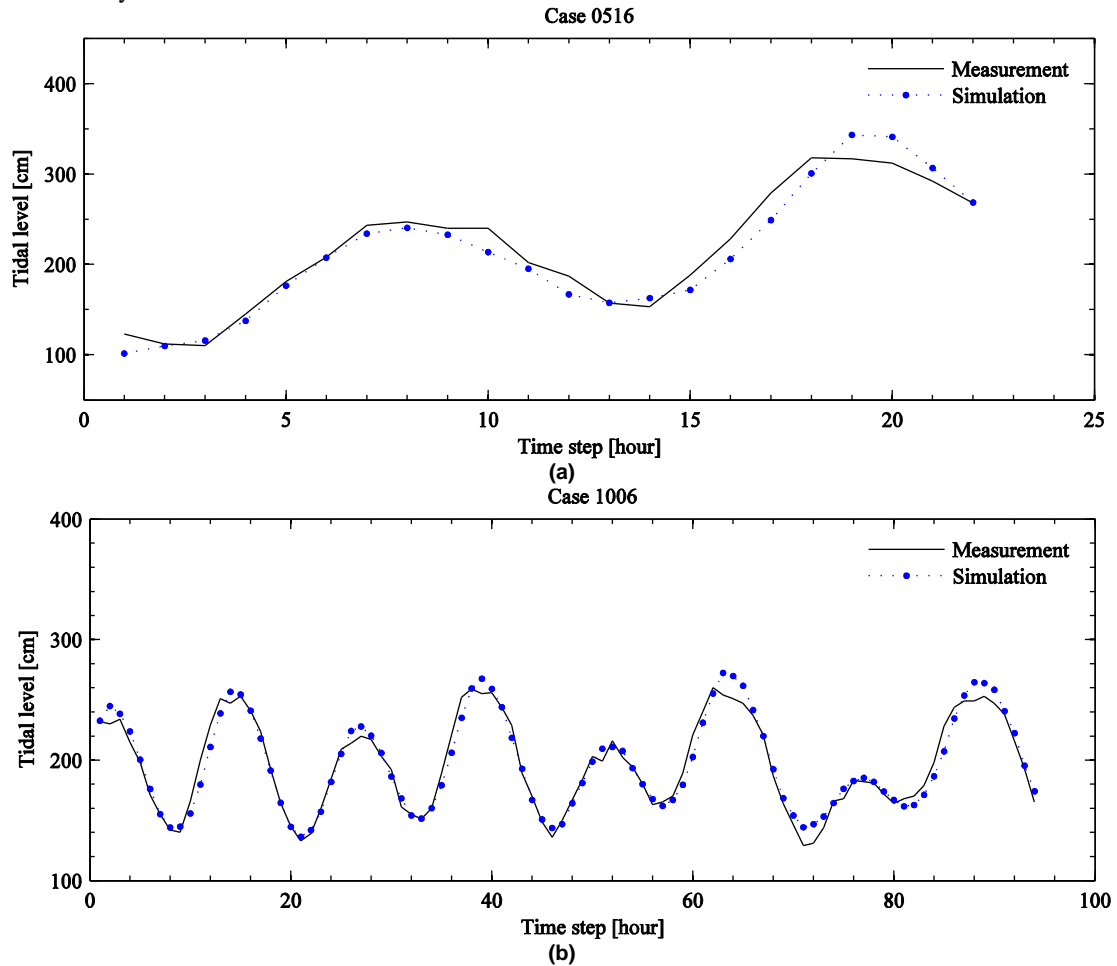


Figure 3. Comparison of the storm tide simulation with measurements for cases with the highest and lowest *RMSE* in the group of the cyclone warning no. 1 as the highest; (a) Case 0516 with *RMSE* = 0.16 m and R^2 = 0.95, (b) Case 1006 with *RMSE* = 0.08 m and R^2 = 0.95.

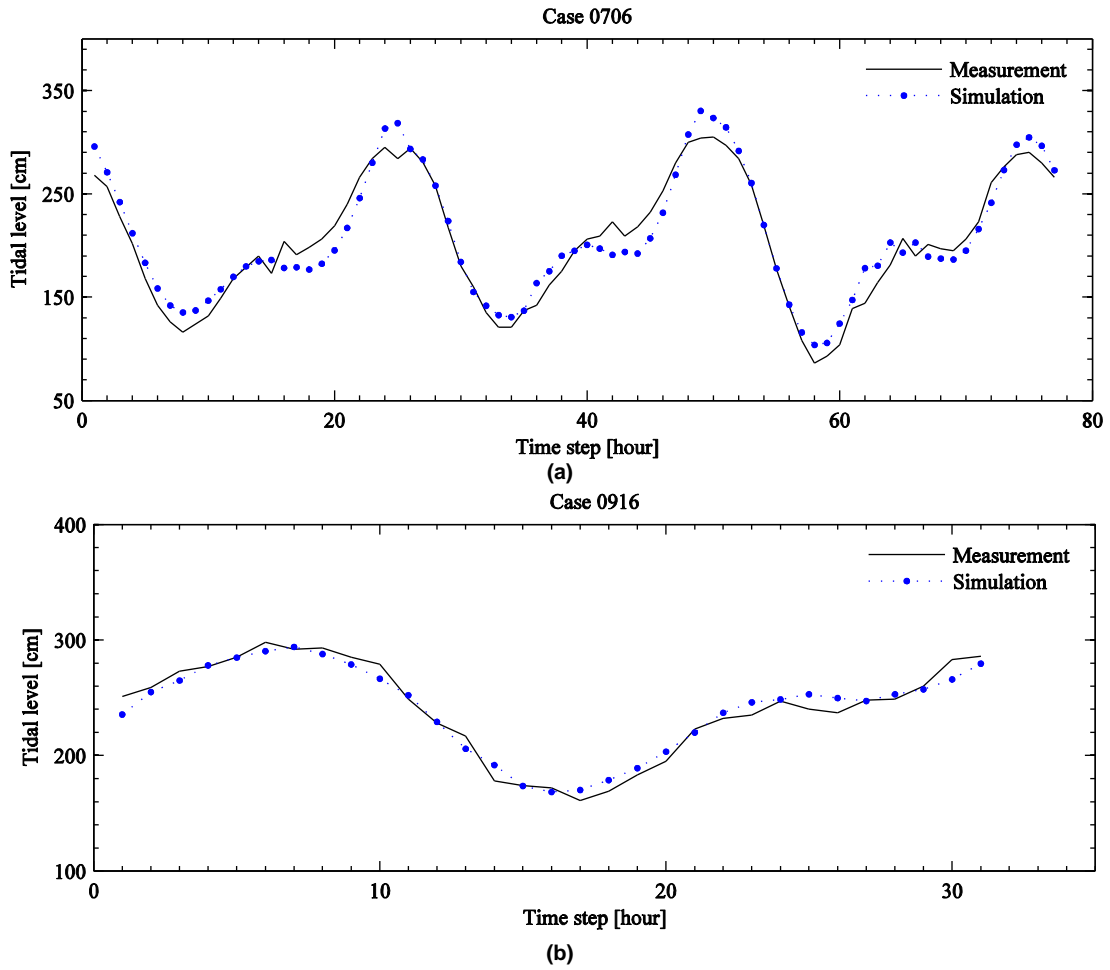


Figure 4. Comparison of the storm tide simulation with measurements for cases with the highest and lowest *RMSE* in the group of the cyclone warning no. 3 as the highest; (a) Case 0706 with *RMSE* = 0.16 m and $R^2 = 0.93$, (b) Case 0916 with *RMSE* = 0.08 m and $R^2 = 0.97$.

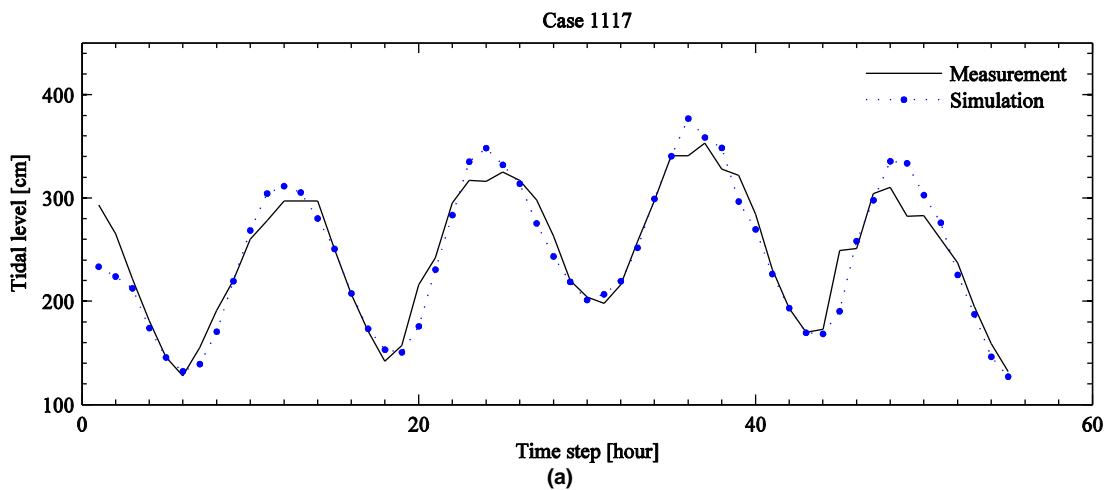


Figure 5. Comparison of the storm tide simulation with measurements for cases with the highest and lowest *RMSE* in the group of the cyclone warning no. 8 as the highest; (a) Case 1117 with *RMSE* = 0.20 m and $R^2 = 0.91$, (b) Case 1213 with *RMSE* = 0.09 m and $R^2 = 0.98$. (Continued on the next page.)

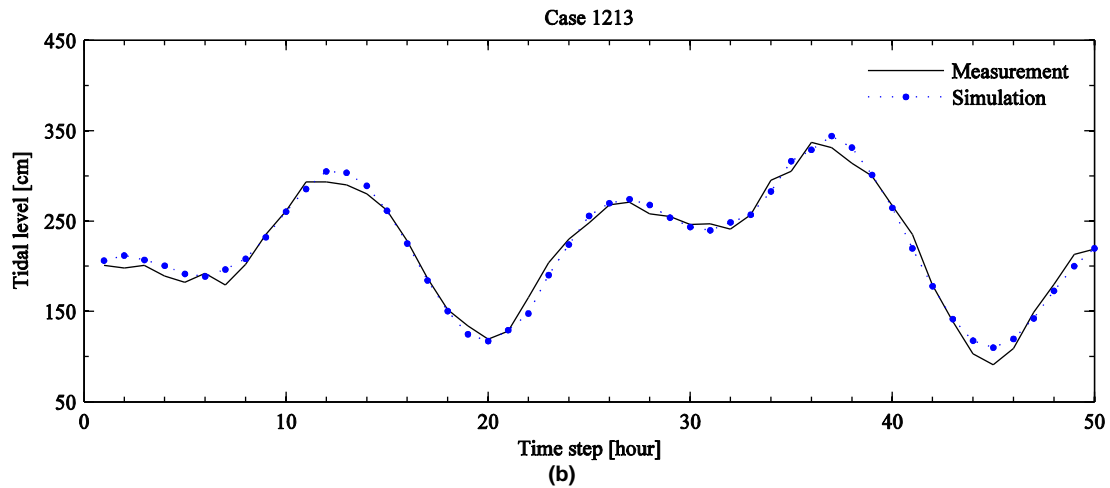


Figure 5. (continued) Comparison of the storm tide simulation with measurements for cases with the highest and lowest $RMSE$ in the group of the cyclone warning no. 8 as the highest; (a) Case 1117 with $RMSE = 0.20$ m and $R^2 = 0.91$, (b) Case 1213 with $RMSE = 0.09$ m and $R^2 = 0.98$.

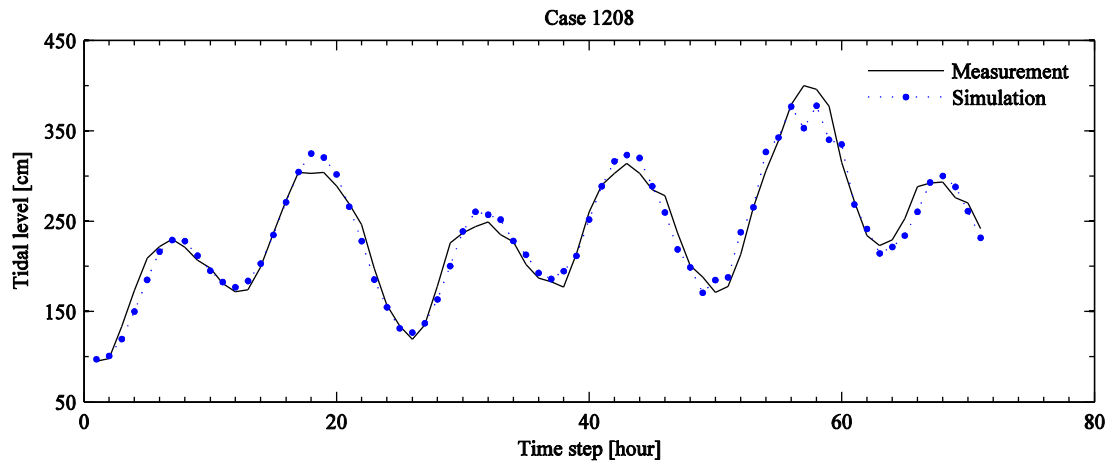


Figure 6. Comparison of the storm tide simulation with measurements for the only case in the group of the cyclone warning no. 9 as the highest; Case 1208 with $RMSE = 0.14$ m and $R^2 = 0.96$.

The direct consequence of storm tide in Macau is flooding of the low-lying area, especially the inner harbor of the city where the tide gauge is installed. Because of this, the Chief Executive Officer of the Macau SAR government in April of 2009 signed an administration order that stipulates the issue of a storm surge warning by SMG when the sea level is expected to exceed road level of the inner harbor, which is at +3.10m from the datum of the tide gauge. With this as the threshold, seventeen out of the forty cases studied here were reported with flooding. For a warning issuing operation, information of two parameters are of great importance. They are the maximum or peak of the storm tide and its arrival time. Performance of the model on the seventeen flooding cases is reviewed by examining results on these two parameters together with values of the overall model simulation $RMSE$ and R^2 as shown in Table 6. The model in general gives good overall simulation in all cases providing a range of $RMSE$ and R^2 between 0.09m to 0.20m and 0.90 to 0.98, respectively. Performance on the peak is first reviewed by finding the difference of the simulated peak level from the corresponding measurement. The absolute difference ranges from 0.01m to 0.25m with a $RMSE$ of 0.15m. These translate to a 0.2% to 7.9% with an average of 3.5%. The model over-estimated the peak level on thirteen cases, of which eight cases are within 5% and five cases are above 5% but below 8%. On the other hand the model only under-estimated the peak level on four cases, all are less than 6%. As for the peak arrival time, the model estimated it to be within one hour from the actual arrival time in fifteen out

of the seventeen cases. The other two cases, the model estimated it to arrive two hours early. The differences in the peak value and its arrival time may be caused by the characteristics of the approaching tropical cyclone. The surge not only depends on how strong the wind is but also the moving path and speed of the cyclone. Effects of the wind have more time to accumulate if the tropical cyclone approaches the coast in a slower rate. Therefore a higher wind surge will result. On the other hand, the wind surge will be lower if the cyclone is approaching in a faster speed since there is less time for the accumulation of wind energy effects. This possible effect is not considered in the present model. However, the final storm tide level will also depend on the tide (spring or neap) that the storm surge rides on. At a coinciding combination of these factors, a storm tide could lead to severe flooding in the low-lying area of the coast.

Table 6. Peak difference of the model (flooding case)

| Cyclone case | Highest cyclone warning issued | Overall performance | | Peak performance | | |
|--------------|--------------------------------|---------------------|-------------|-----------------------------|----------------------------|----------------------------|
| | | RMSE (m) | R^2 | Peak arrival time diff. (h) | Peak tidal level diff. (m) | Peak tidal level diff. (%) |
| 0516 | 1 | 0.16 | 0.95 | 1 | 0.25 | 7.9 |
| 0518 | 3 | 0.12 | 0.94 | -2 | -0.01 | 0.2 |
| 0601 | 3 | 0.11 | 0.98 | 1 | 0.18 | 5.3 |
| 0606 | 8 | 0.14 | 0.90 | -2 | 0.05 | 1.4 |
| 0609 | 1 | 0.12 | 0.97 | 1 | 0.24 | 7.1 |
| 0713 | 1 | 0.12 | 0.97 | 1 | 0.22 | 6.8 |
| 0809 | 8 | 0.12 | 0.95 | -1 | -0.01 | 0.3 |
| 0814 | 8 | 0.16 | 0.98 | -1 | 0.08 | 1.8 |
| 0904 | 3 | 0.12 | 0.97 | 1 | 0.02 | 0.7 |
| 0907 | 8 | 0.11 | 0.97 | 1 | 0.01 | 0.4 |
| 0915 | 8 | 0.16 | 0.96 | 1 | 0.19 | 4.5 |
| 1013 | 1 | 0.12 | 0.92 | -1 | 0.04 | 1.2 |
| 1108 | 3 | 0.12 | 0.97 | 1 | 0.11 | 3.2 |
| 1117 | 8 | 0.20 | 0.91 | -1 | 0.24 | 6.7 |
| 1119 | 3 | 0.13 | 0.93 | -1 | -0.12 | 3.3 |
| 1208 | 9 | 0.14 | 0.96 | 1 | -0.22 | 5.6 |
| 1213 | 8 | 0.09 | 0.98 | 1 | 0.07 | 2.1 |
| | Min. | 0.09 | 0.90 | Max. | RMSE | Average |
| | Max. | 0.20 | 0.98 | 2 | 0.15 | 3.5 |

Out of the seventeen flooding cases, two are considered extreme scenarios. They are case 0814 which gave the most severe flooding to the inner harbor region among all, and case 1208 which had the highest tropical cyclone warning (no.9) issued. They are reviewed in further details. Figure 7 shows the temporal variation of the storm tide given by the model with measurements for case 0814. In this scenario, the cyclone period lasted for 43 hours, and the highest warning issued was no. 8. The *RMSE* and R^2 of the simulation are 0.16m and 0.98, respectively. The model captures the flood and ebb of the storm tide well. The simulated peak value is 4.68m that is only 0.08m (1.8%) higher than the measured peak. The peak arrival time given by the model is at one hour earlier than the measurement. For case 1208, the model simulation and measurements have already been shown in Figure 6. This is the only case in this study had the cyclone warning no. 9 issued, which is the highest among all. It lasted for 71 hours. The *RMSE* and R^2 of the simulation are 0.14m and 0.96, respectively. The model captures the floods and ebbs of the storm tide in these 3 days very well. The simulated peak value is 3.78m that is 0.22m (5.6%) lower than the measured peak. The peak arrival time given by the model is at 1 hour later than the measurement. In short, the model performs very well in simulating the storm tide occurred in Macau even for the extreme scenarios that gave severe flooding.

CONCLUSION

In this study, Kalman filter based empirical dynamic model is proposed for a local storm tide simulation (*STS*) with four input factors: the predicted astronomical tide, measured atmospheric pressure, wind speed and direction. The model was tested with forty tropical cyclone cases in Macau. Results concluded that it can handle all cases of different cyclone strength (warning no.1 to no.9) well. Within the forty studied cases, seventeen were reported with flooding. Further analysis of the model simulation on the peak level value and its arrival time for these cases showed that it works well even for the extreme scenarios. Even the present model is developed based on its application in Macau, it

should be stressed that the proposed technique is general. It is applicable to other regions with slight adjustment of the model expression. In addition, the developed simulation model can be readily applied to the operational flood forecasting if good meteorological forecasts are available.

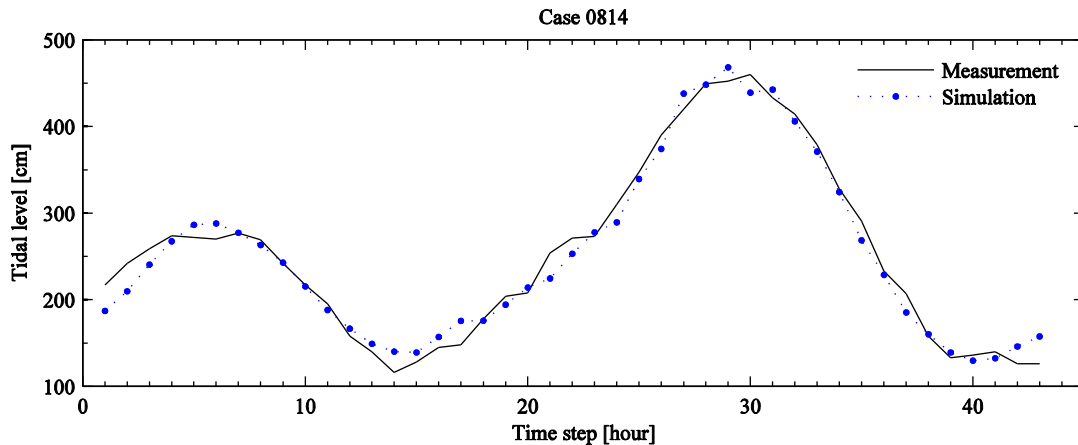


Figure 7. Comparison of the storm tide simulation with measurements for case 0814 with $RMSE = 0.16m$ and $R^2 = 0.98$; the highest cyclone warning issued was no. 8.

ACKNOWLEDGMENTS

This work is supported by the research committee (MYRG2014-00038-FST) of the University of Macau and the Science and Technology Development Fund (079/2013/A3) of the Macau SAR Government. The Marine and Water Bureau, and the Meteorological and Geophysical Bureau of Macau SAR are thanked for supplying the tide gauge data and meteorological data.

REFERENCES

- Chao, K.M., K.I. Hoi, K.V. Yuen, and K.M. Mok. 2012. Adaptive Modeling of the Daily Behavior of the Boundary Layer Ozone in Macau, *ISRN Meteorology*, 2012, Article ID 434176.
- Choi, I.C., K.M. Mok, and S.C. Tam. 2002. Solving Harmonic Sea-Level Model with Kalman Filter: A Macau case Study, *Carbonate Beaches 2000, Florida, United States, 5-8 December 2000*, 38-52.
- Hoi, K.I., K.V. Yuen, and K.M. Mok. 2013. Improvement of the multilayer perceptron for air quality modeling through an adaptive learning scheme, *Computer & Geosciences*, 59, 148-155.
- Lee, T.L. 2006. Neural network prediction of a storm surge, *Ocean Engineering*, 33, 483-494.
- Rajasekaran, S., S. Gayathri, and T.L. Lee. 2008. Support vector regression methodology for storm surge predictions, *Ocean Engineering*, 35, 1578-1587.
- Wong, C.F., and K.W. Li. 2007. Sea level anomalies in Hong Kong due to strong monsoon (in Chinese), *The 21st Guangdong-HongKong-Macau Seminar on Meteorological Science and Technology, Hong Kong, China, 24-26 January 2007*, 21pp.
- Wong, W.T., and C.F. Wong. 2008. Storm Surge Forecast in Hong Kong (in Chinese), *Technical Seminar on Marine Hazards Forecasting, Beijing, China, 4-5 December 2008*, 10pp.
- Yuen, K.V. 2010. *Bayesian Methods for Structural Dynamics and Civil Engineering*. John Wiley & Sons (Asia) Pte, Ltd., Singapore, 294pp.